ent, resulting in a rapid reduction in $\theta$, before the effects due to the adverse gradient near the outlet take over. The $C_f$ remains well positive throughout the contraction, thus indicating that separation is not predicted for this particular design. The results from the two techniques are seen to compare favorably, especially for the region near the contraction outlet. Since the program for Thwaites method is relatively easy to obtain and use,[6] all of the boundary-layer data presented below were computed using this method.

In order to validate the proposed computational scheme, the boundary-layer properties in four contractions installed on blower-driven wind tunnels (Table 1) were calculated and compared with actual measurements. The wall shapes for the four contraction sections are plotted in normalized coordinates in Fig. 3. Two of the wall shapes were based on a fifth-order polynomial, while the other two were designed "by eye" following the guidelines given in Ref. 1. Note that for all four contractions investigated, the nondimensional geometric parameters are similar; the contraction ratio is about 8, the length to inlet height ratio is about 1, and the cross-sectional aspect ratio at the exit is about 5.

For all four contraction shapes, the computations predicted an attached boundary layer along the entire length. The measured values of the boundary-layer momentum thickness at the exit of the contractions are compared with those predicted by Thwaites' method in Table 2. The comparisons are made along the wind-tunnel centerline at a short distance (typically less than 15 cm) downstream of the contraction exit. The predicted values of the momentum thickness for all four cases are within about 10% of the measured ones; the typical measurement repeatability was within 1%. The predicted values generally are lower than the measured ones, presumably due to the generation of weak secondary flows along the contraction walls,[8] which tend to thicken the boundary layer along the tunnel centerline. Note that the maximum error between the predictions and experiments occurs for wind tunnel A, which also has the maximum three-dimensionality in the contraction geometry. The agreement between predictions and measurements for all the other boundary-layer properties was comparable and details are given in Ref. 3.

## Conclusions

A scheme is proposed for the prediction of boundary-layer development in small, low-speed contraction sections. The wall pressure distributions, and hence the wall velocity distributions, are first calculated using a three-dimensional potential flow method. Although a panel method was used in this investigation, in principle, any potential flow solver should be acceptable. Once the wall velocities have been obtained, the boundary-layer behavior can be adequately calculated, rather than relying on some separation criterion. For the family of contractions discussed in this Note, the assumption of a laminar boundary layer originating at the contraction entrance and remaining laminar in passage through it seems justified. The measured boundary-layer momentum thicknesses at the exit of four existing contractions, two of which were three-dimensional, were found to lie within 10% of the predicted values, with the predicted values generally lower. The present results indicate that the relatively simple Thwaites method is probably adequate for most purposes. If the prediction accuracy of within 10% on $\theta$ is acceptable, then the present results also suggest that an iterative process, accounting for the boundary-layer displacement thickness, is not necessary.

## Acknowledgments

This work was supported by the Fluid Dynamics Research Branch, NASA Ames Research Center under Grant NCC-2-294. We would like to thank our colleagues at NASA Ames Research Center for many helpful comments.

## References

[1]Mehta, R. D. and Bradshaw, P., "Design Rules for Small Low Speed Wind Tunnels," *Aeronautical Journal,* Vol. 83, No. 827, Nov. 1979, pp. 443-449.

[2]Bradshaw, P., "Effects of Streamline Curvature on Turbulent Flow," AGARDograph 169, Aug. 1973.

[3]Bell, J. H. and Mehta, R. D., "Contraction Design for Small Low-Speed Wind Tunnels," Dept. of Aeronautics and Astronautics, Stanford Univ., Stanford, CA, JIAA Rept. TR-84, April 1988; also NASA-CR 177488, Aug. 1988.

[4]Stratford, B. S., "The Prediction of Separation of the Turbulent Boundary Layer," *Journal of Fluid Mechanics,* Vol. 5, Pt. 1, Jan. 1959, pp. 1-16.

[5]Mehta, R. D., "Turbulent Boundary Layer Perturbed by a Screen," *AIAA Journal,* Vol. 23, Sept. 1985, pp. 1335-1342.

[6]Cebeci, T. and Bradshaw, P., *Momentum Transfer in Boundary Layers,* Hemisphere, New York, 1977.

[7]Murphy, J. D. and King, L. S., "Airfoil Flow-Field Calculations with Coupled Boundary-Layer Potential Codes," *Proceedings 2nd Conference on Numerical and Physical Aspects of Aerodynamic Flows,* California State Univ., Long Beach, CA, 1983.

[8]Mokhtari, S. and Bradshaw, P., "Longitudinal Vortices in Wind Tunnel Wall Boundary Layers," *Aeronautical Journal,* Vol. 87, June/July 1983, pp. 233-236.

# Motion and Deformation of Very Large Space Structures

Ramesh B. Malla*
*University of Connecticut, Storrs, Connecticut*
and
William A. Nash† and Thomas J. Lardner†
*University of Massachusetts, Amherst, Massachusetts*

## Introduction

THE effects of various space environmental factors (such as gravitational forces, radiation heating, radiation pressure, space drag, and particle impact) on space structures have long been realized and studied by numerous investigators in past for small-sized space structures (for example, see reference list in Ref. 1). The deployment of very large flexible lightweight structures in space, which have characteristic dimensions of several kilometers operating at altitudes of 200-35,900 km above the Earth's surface, gives rise to a number of new and significant problem areas that may or may not have been associated with smaller systems.

This Note presents a theoretical development of the equations of motion of a very large axially flexible structure orbiting the Earth with planar motion in a general noncircular orbit. With the help of these equations of motion, it is anticipated that effects of many disturbances can be investigated on large space structures' orbital motion, attitude motion, and axial deformation (length). As an application of the equations of motion, the effects of the orbit eccentricity are studied on the coupled orbital, attitude, and axial motion of a large space structure under the influence of the Earth's gravitational forces.

Received Oct. 10, 1987; revision received April 27, 1988. 

*Visiting Assistant Professor, Department of Civil Engineering.
†Professor, Department of Civil Engineering.

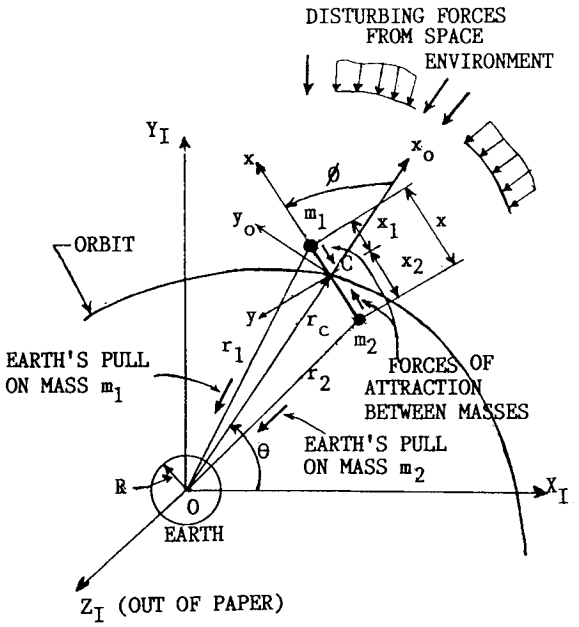


**Fig. 1 Large orbiting structure in space environment.**

## Theoretical Development

The geometric configuration under consideration represents a very large space structure consisting of two point masses, $m_1$ and $m_2$, connected by an axially flexible link structure that moves in a general noncircular orbit around the spherical Earth of radius $R$ with center at $O$ (Fig. 1). The mass of the link structure is considered to be lumped at the two ends. This dumbbell structure is assumed to move in the orbital plane (coplanar motion). It is also assumed that the orbit of the structure is defined by the motion of its center of mass $C$.

The generalized coordinates of the problem are 1) the radial distance $r_c$ between the center of the Earth and the center of mass of the space structure, 2) the angle $\theta$ describing the sweep of the radial line $r_c$ in the plane of motion, 3) the distance $x$ between the two dumbbell masses $m_1$ and $m_2$, and 4) the angle $\phi$ between the local vertical line $OC$ and the line joining the two masses.

### Kinetic Energy

The total kinetic energy of the system with respect to Earth-fixed axes $X_I$, $Y_I$, $Z_I$ (Fig. 1) can be determined readily[1] as:

$$K_E = \tfrac{1}{2}\{m[\dot{r}_c^2 + (r_c\dot{\theta})^2] + \bar{m}[\dot{x}^2 + x^2(\dot{\theta}+\dot{\phi})^2]\} \qquad (1)$$

where $m = m_1 + m_2$, the reduced mass, $\bar{m} = (m_1 m_2)/m$, and the dot on top of a character represents the time derivative of the corresponding quantity.

### Potential Energy

The total potential energy of the conservative forces acting on the system is given by[1]

$$P_E = -\mu\left(\frac{m_1}{r_1} + \frac{m_2}{r_2}\right) - G\frac{m_1 m_2}{x} + U_e \qquad (2)$$

where $\mu = gR^2$ is a constant quantity in which $g$ is the acceleration due to gravity at the Earth's surface, $r_1$ and $r_2$ the distances of the mass centers of masses $m_1$ and $m_2$ from the center of the Earth, respectively, $G$ the universal gravitational constant, and $U_e$ the strain energy. The first and the second terms in Eq. (2) represent potential energies due to the Earth's pull on the two end masses $m_1$ and $m_2$, respectively, and the third term potential energy due to the attractive forces between them.

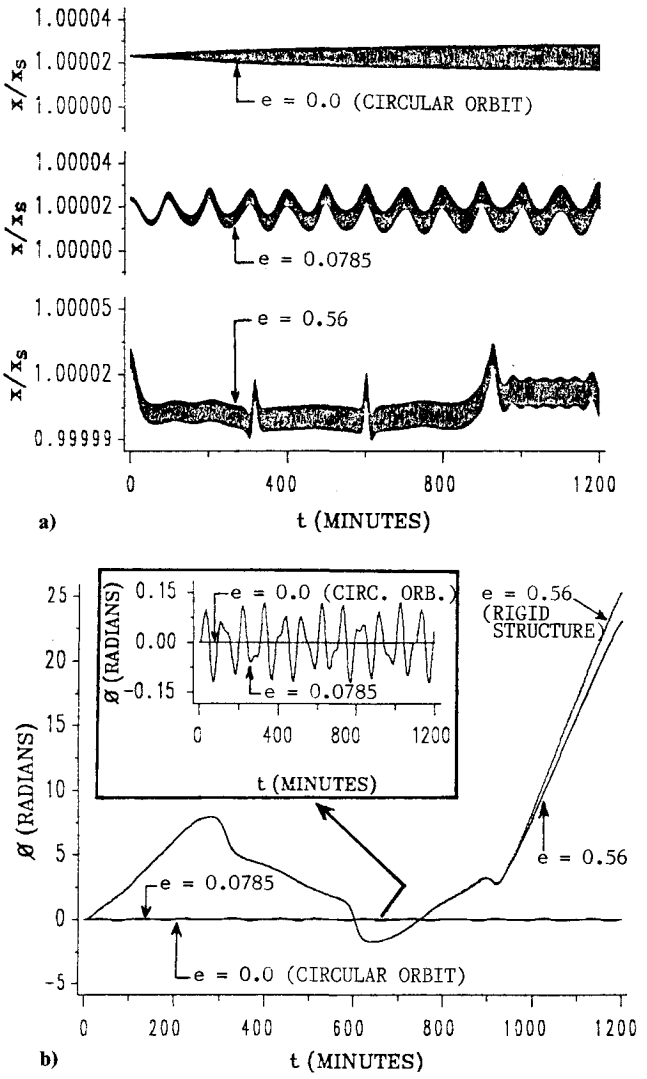


**Fig. 2 Variations of a) axial length $x$ and b) attitude angle $\phi$ of a space structure.**

### Equations of Motion

Using Lagrange's procedure, the equations of motion of the space structure can be obtained as[1]

$$m\ddot{r}_c - mr_c\dot{\theta}^2 + \mu\left[\frac{m_1(r_c + x_1\cos\phi)}{r_1^3} + \frac{m_2(r_c + x_2\cos\phi)}{r_2^3}\right] = Q_r \qquad (3a)$$

$$mr_c(r_c\ddot{\theta} + 2\dot{\theta}\dot{r}_c) - \bar{m}\mu\left[\frac{(-1)}{r_1^3} + \frac{1}{r_2^3}\right]xr_c\sin\phi = (Q_\theta - Q_\phi) \qquad (3b)$$

$$\bar{m}\ddot{x} - \bar{m}x(\dot{\theta}+\dot{\phi})^2 + \bar{m}\mu\left[\frac{(x_1 + r_c\cos\phi)}{r_1^3} + \frac{m_2(x_2 + r_c\cos\phi)}{r_2^3}\right] + \frac{Gm_1m_2}{x^2} + \frac{\partial U_e}{\partial x} = Q_x \qquad (3c)$$

$$\bar{m}[x^2(\ddot{\theta}+\ddot{\phi}) + 2x\dot{x}(\dot{\theta}+\dot{\phi})] + \bar{m}\mu\left[\frac{(-1)}{r_1^3} + \frac{1}{r_2^3}\right]xr_c\sin\phi = Q_\phi \qquad (3d)$$

where $Q_r$, $Q_\theta$, $Q_x$, and $Q_\phi$ are generalized forcing functions corresponding to the coordinates $r_c$, $\theta$, $x$, and $\phi$, respectively. The differential equations of motion thus derived are coupled and nonlinear. The transverse oscillations of the structure is not included in the derivation of the equations of motion.

## Applications

To determine the effects of various external environmental factors on a space structure's motions and deformation, the equations of motion need to be solved with appropriate expressions for the strain energy $U_e$ and forcing function terms $Q_r$, $Q_\theta$, $Q_x$, and $Q_\phi$.

As an application of the equations of motion, the effects of the Earth's gravitational forces are studied on a space structure's motion and deformation. Here, we have, $Q_r = 0$, $Q_\theta = 0$, $Q_x = 0$, and $Q_\phi = 0$. For an axially flexible structure, within linear elastic deformation, the strain energy corresponding to axial force can be obtained from $U_e/dx = K_a\ (x - x_s)$, where $K_a$ is the longitudinal stiffness of the structure and is given by $K_a = A_{cs}E/x_s$ (in which $A_{cs}$ and $E$ are the area of the cross section and modulus of elasticity of the structure, respectively). $x_s$ is the static (reference) length of the dumbbell structure. The equations of motion are solved by a numerical integration method using a fifth- and sixth-order Runge-Kutta-Verner method.

### Physical Model and Initial Conditions

A tetrahedral truss configuration has been selected to represent a large space system. The masses of the truss and substructures erected on it are considered to be lumped at the two ends of the structure, giving a dumbbell-shaped model. The equivalent mechanical properties of the truss system are determined[1] and are along with other constant parameters: $G = 8.64432 \times 10^{16}$ km$^4$/N·min$^4$, $g = 35.316$ km/min$^2$, $R = 6374.33$ km, $x_s = 1.0$ km, $A_{cs} = 2.4495 \times 10^{-4}$ km$^2$, $E = 6.689496 \times 10^{10}$ N/km$^2$, and $m_1 = m_2 = 5.0 \times 10^5$ N·min$^2$/km.

The initial conditions in $r_c$ is 6574.33 km (200 km altitude from the surface of the Earth). Circular and elliptical orbits are considered to study the effects of orbit eccentricity on the structure's motion and deformation. The initial values of the length $x$ equal to 1.000023 km and angular velocity $\dot{\theta}$ equal to 0.07106292041142 rad/min are determined from the equilibrium state of the space structure in a circular orbit at 200 km altitude.[1] The orbital period of this circular orbit is approximately 88.4 min. Two elliptical orbits are considered—one with the initial orbital angular velocity $\dot{\theta}_0$ equal to 0.0738 rad/min, giving a small orbit eccentricity ($e = 0.0785$), and the other with $\dot{\theta}_0$ equal to 0.08883 rad/min, giving a fairly large orbit eccentricity ($e = 0.56$). The orbital periods of the small and large eccentric orbits are approximately 100 and 305.6 min, respectively. The initial values in $\theta$, $\phi$, $\dot{r}_c$, $\dot{x}$, and $\dot{\phi}$ are set equal to zero.

### Results

The effects of the orbit eccentricity on the structure's axial length are apparent in Fig. 2a where two different types of oscillation in $x/x_s$ can be seen. One is the fine, closely spaced, small-amplitude oscillation in $x$, which exists even in zero eccentric orbit (circular orbit). Such a small oscillation in $x/x_s$ may be due to the possible oscillations in $\phi$ because of some round-off and truncation errors while computing the initial values of $x$ and $\dot{\theta}$. The second kind of oscillation in $x/x_s$, which has a larger amplitude and longer period of oscillation, is mainly due to the orbit eccentricity. For the small (slightly) eccentric orbit ($e = 0.0785$), the oscillation in $x/x_s$ is sinusoidal. For the large eccentric orbit ($e = 0.56$), a beat-type resonant phenomenon can be observed (Fig. 2a).

Figure 2b shows that an increase in the eccentricity of an orbit introduces larger liberation in the attitude motion $\phi$. For the slightly eccentric orbit, $\phi$ oscillates about the local vertical with varying amplitude and period of oscillation (Fig. 2a, inset). For the large eccentric orbit, the dumbbell is ultimately observed to be tumbling continuously. For such a large eccentric orbit, computer simulation results for the same size system treated as rigid and flexible bodies show that, in an earlier part of the orbital motion, the difference in the amplitudes of oscillation in $\phi$ for these two type of systems is very small. On the other hand, in the latter part of the motion, the rigid structure is observed to have the greater tendency toward tumbling (Fig. 2b).

It should be mentioned here that the application of the equations of motion is not limited to the study of gravitational force effects only. The application of the equations can be extended to study the effects of many other environmental factors (e.g., thermal, radiation pressures, etc.) on a space structure. For example, on an axially flexible unrestrained structure, thermal effects can be investigated when it is realized that the external forcing functions $Q_r$, $Q_\theta$, $Q_x$, and $Q_\phi$ are zero and the strain energy $U_e$ can be expressed in terms of the temperature variation of the structure.[1,2]

## Conclusions

Using the equations of motion developed in the present study, an investigation of effects of the orbit eccentricity on the motion and deformation of a large space structure under the action of the Earth's gravitational forces shows that an increase in orbit eccentricity greatly disturbs the attitude motion of the space structure. For highly eccentric orbits, the structure may tumble continuously. The orbit eccentricity, however, produces only small-magnitude of structural deformation.

## Acknowledgments

This study has been supported in part by the Air Force Office of Scientific Research under Grant AFSOR-83-0025.

## References

[1]Malla, R. B., "Dynamic and Thermal Effects in Very Large Space Structures," Ph.D. Thesis, Univ. of Massachusetts, Amherst, Sept. 1986.

[2]Malla, R. B., Nash, W. A., and Lardner, T. J., "Thermal Effects on Very Large Space Structures," *ASCE Journal of Aerospace Engineering*, Vol. 1, No. 3, July 1988, pp. 171-190.